PCCP

PAPER

View Article Online
View Journal | View Issue

Published on 03 September 2015. Downloaded by Universiteit Utrecht on 13/11/2015 09:02:06.

Cite this: *Phys. Chem. Chem. Phys.*, 2015, **17**, 26270

DFT+U studies of Cu doping and p-type compensation in crystalline and amorphous ZnS

Hieu H. Pham,[a] Gerard T. Barkema[b] and Lin-Wang Wang*[a]

Received 5th August 2015,
Accepted 2nd September 2015

DOI: 10.1039/c5cp04623h

www.rsc.org/pccp

Zinc sulfide is an excellent candidate for the development of a p-type transparent conducting material that has great demands in solar energy and optoelectronic applications. Doping with Cu is one potential way to make ZnS p-type while preserving its optical transparency for the solar spectrum; however, this is limited by the extremely low solubility of Cu in ZnS and charge compensation mechanisms that eliminate the p-type characteristics. These mechanisms are different in crystalline (c-ZnS) and amorphous structures (a-ZnS), leading to different tendencies of doping Cu in these two ZnS phases, as well as the feasibility to form the p-type material. In this work, we have carried out fundamental studies of Cu doping in both c-ZnS and a-ZnS, using the continuous random network model and density functional theory with Hubbard's energy correction (DFT+U). The formation of a complex that contains two Cu_{Zn} and one S vacancy is highly favorable in both phases. The local environment of this charge-compensated Cu complex obtained by DFT calculations agrees well with the previous EXAFS measurements. The incorporation of Cu into a-ZnS, on the one hand, is more tolerable compared to its crystal counterparts (zincblende), indicating possible higher Cu concentration. On the other hand, there is also another intrinsic mechanism to compensate the p-type characteristics in a-ZnS: the formation of the covalent S–S "dumbbell" units. This reconstruction of the local structure to form a S–S bond could occur spontaneously, thus making the p-type doping for ZnS challenging even in the amorphous phase.

1. Introduction

Transparent conducting materials (TCMs) play an essential role in the performance of many devices for electronic applications, including photovoltaics, light emitting diodes and transparent thin film transistors.[1,2] However, only n-type TCMs have been successfully developed to date for commercial use; for example, impurity-doped zinc oxide, indium oxide and tin oxide are among the most popular ones.[3] The development of p-type TCM thin films, including oxides with delafossite structure (*e.g.* $CuMO_2$ and $AgMO_2$, M = trivalent cation) and spinel structure (*e.g.* $NiCo_2O_4$), mixed oxides, (*e.g.* In_2O_3–Ag_2O, SnO_2), non-oxide materials (*e.g.* $BaCu_2S_2$), *etc.*,[2,4–6] is still an active research area since the first report of high p-type conductivity in $CuAlO_2$.[7] In fact, developing p-type TCMs is difficult because many transparent materials have a relatively low valence band edge, which makes it difficult to be doped as p-type due to either the doping limit rules[8,9] or compensation mechanisms.[10] But for many junction device applications, both n-type and p-type TCMs are essential.[7,11,12] ZnS-based materials have been extensively studied and have shown their potential for this purpose.[13–16] They have a suitable band gap that guarantees no absorption in the visible range, however exhibit a limited conductivity. Copper sulfide materials Cu_xS, on the contrary, are highly conductive but not transparent to wavelengths in the solar spectrum, due to their small band gap.[17] Many attempts have been made to dope Cu into the ZnS matrix to improve the conductivity.[12,18] The challenge here partially lies in the significant dissimilarity in the crystal structures of zinc sulfide and copper sulfide that makes their alloys difficult to form. As a result, Cu is only soluble in ZnS up to a concentration of about 400 ppm.[19] Instead, Cu would be found either near the surface of the ZnS nanoparticles or in phase separated CuS or Cu_2S precipitates.[19–21] One common technique is to use co-activators such as Al^{3+}, Ga^{3+}, In^{3+}, Cl^- or Br^- for charge compensation to stabilize Cu in the host lattice.[22] Besides the difficulty in doping ZnS with Cu, another problem is the formation of compensating defects (or defect complexes), which can kill the charge carriers (holes). Another issue that has drawn attention is the formation of highly disordered phases, *i.e.* amorphous structures. The dopability in crystalline and amorphous structures could be drastically different, so are their typical charge compensation mechanisms. In general, the introduction of holes depends on multiple factors; including the formation and ionization energy of charge producing defects, as well as the formation energy of charge

[a] *Joint Center for Artificial Photosynthesis and Materials Sciences Division Lawrence Berkeley National Laboratory, Berkeley, California 94720, USA. E-mail: lwwang@lbl.gov*
[b] *Theoretical Physics, Utrecht University, Leuvenlaan 4, 3584 CE Utrecht, The Netherlands*

 This journal is © the Owner Societies 2015

Published on 03 September 2015. Downloaded by Universiteit Utrecht on 13/11/2015 09:02:06.

killing defects.[23] Therefore, it would be interesting to know whether it is more favorable or challenging to form p-type ZnS in amorphous structure, in regard to both Cu doping limits and charge balance mechanisms. In this work, we will investigate the structural characterization, electronic properties and several typical p-type compensation models of Cu doping in both crystalline (zincblende c-ZnS) and amorphous (a-ZnS) phases, using first principles calculations.

Relative to the crystalline counterparts, the amorphous structures are highly favorable for solar cells and flat-panel display applications, due to the cost-effectiveness of growth and deposition techniques as well as their ability to form a smooth interface with large-area substrates of different lattice constants.[24] In fact, the low-temperature synthesis of amorphous materials has become standard and their use is ubiquitous. It was shown that the amorphous films could exhibit superior properties and significantly improve the performance of many photoelectric devices.[24–27] Additionally, experimental studies have suggested that the nanoparticles or quantum dots, which have been extensively investigated for next-generation solid-state lighting applications, favorably adopt the core–shell structure, and the shell is often composed of the amorphous phase.[27–30] While the tendency of forming p-type c-ZnS and compensation mechanisms that eliminate the p-type characteristics have been investigated both experimentally and theoretically,[12,31] the situation in a-ZnS is rather unknown.

The study of the amorphous materials is nontrivial because the definition of a realistic amorphous structure could be ambiguous. Here we have employed a continuous random network approach (CRN) to construct well-relaxed atomic configurations of a model amorphous ZnS. The electronic structure of this Cu-doped ZnS system, together with its zincblende counterpart, is then investigated by density functional theory (DFT), including the hybrid functional (HSE06)[32] and the GGA+U.[33] The Cu doping and alloying in wurtzite ZnS have also been studied by our group through *ab initio* calculations.[12] It was found that the most predominant defect is the Cu_{Zn}^{-} antisite when the Fermi energy is above the valence band edge. However, this previous study has not addressed the issue of the amorphous structure and charge-compensated complexes such as $V_SCu_{Zn}Cu_{Zn}$. Those are the issues we investigate in this work and we find that: (i) despite the structural disorder, the CRN amorphous ZnS model has no mid-gap states (even though its band gap is narrower than its crystal counterpart); (ii) the formation energy of the Cu dopant in the amorphous ZnS is significantly lower than that in the zincblende system, which suggests a higher solubility of Cu in the amorphous phase; (iii) in both c-ZnS and a-ZnS, the formation of the S vacancy (V_S) adjacent to Cu_{Zn} is thermodynamically favorable (by several eV), compared to the separated configurations. In this context, the Cu–S and Zn–S bond distances are reduced as Cu and Zn are pushed away from the S vacancy and towards three remaining S nearest neighbors. This agrees with experimental observation using the EXAFS technique;[31] (iv) in the amorphous structure, a hole killer upon Cu doping could be prominent: the formation of covalent S–S ''dumbbell'' units, which are similar to those in covellite CuS and pyrite-type Cu_2S structures.[34,35]

2. Computational details

Currently the best approach for the generation of well-relaxed covalent amorphous semiconductors and glasses is the CRN approach of Wooten, Winer and Weaire.[36] Starting from the crystalline diamond structure, local bond switches rapidly transform it into a low-strain amorphous structure free of coordination defects. In this work, the CRN approach, adapted to generate binary alloys,[37] was used to generate a number of initial a-ZnS structures containing between 64 and 200 atoms. The obtained systems (amorphous) were then used for further atomic relaxation by first-principles calculations.

Density functional theory (DFT),[38] as implemented in the Vienna *ab initio* Simulation Package (VASP),[39] was employed to perform first-principles calculations. Most calculations used the electron projector-augmented wave methods[40] with the PBE generalized gradient approximation (GGA) exchange–correlation,[41] plus on-site Zn and Cu d state U corrections (DFT+U, or say GGA+U),[33] otherwise noted. A plane-wave cut-off of 450 eV was used and the magnetic moment was accounted for by performing spin-polarized energy calculations. The values of U = 7.0 and 6.0 were used for the Coulomb corrections to the Zn and Cu 3d states, respectively, which have shown to reproduce well the electronic structure and ground-state properties of ZnS and Cu_2O.[42–44] For the k-space sampling, we used a 3 × 3 × 3 Monkhorst–Pack grid[45] for the 64-atom supercells (both c-ZnS and a-ZnS). For hybrid calculations (HSE06), a 2 × 2 × 2 grid was used.

The formation energy of Cu substitution (Cu replacing Zn) with charge state q is calculated as follows:[46]

$$\Delta H(\mathrm{Cu^q}) = E(\mathrm{Cu^q}) - E(\mathrm{clean}) - (E_{\mathrm{Cu}} + \Delta\mu_{\mathrm{Cu}}) + (E_{\mathrm{Zn}} + \Delta\mu_{\mathrm{Zn}}) + q(\varepsilon_{\mathrm{VBM}} + E_{\mathrm{F}} + \Delta\nu) \quad (1)$$

where $E(\mathrm{Cu^q})$ and E(clean) are the total energies of the supercells with and without the defect (Cu substitution). $\Delta\mu_{\mathrm{Cu}}$ and $\Delta\mu_{\mathrm{Zn}}$ are the elemental chemical potentials of Cu and Zn, referenced to the DFT elemental energy E_{Cu} and E_{Zn} of their ground states (we used the crystal structures of face-centered cubic Cu and hexagonal-closed pack Zn). For simplicity and the purpose of comparison between the crystalline and amorphous models, we assume the metals in their rich conditions, *i.e.* $\Delta\mu$ = 0 for both Cu and Zn (the formation energy difference between c-ZnS and a-ZnS will not depend on these $\Delta\mu$ values). E_{F} is the Fermi energy level referenced to the valence band maximum (VBM) eigenenergy of the bulk ZnS system, and $\varepsilon_{\mathrm{VBM}}$ is the VBM eigenenergy of the bulk system when the averaged Hartree potential is set to zero. The term $\Delta\nu$ is added for the correction of the electrostatic potential caused by the limited size of the supercell, obtained from the shifting of the 1s core-level energy of a Zn atom (located far away from the defect site) between the neutral impurity and charged cases. A similar procedure was adopted for the calculation of the S vacancy, in which the sulfur-6 structure was used as the ground state E_S. The values are presented for S poor conditions, *i.e.* $\Delta\mu_{\mathrm{S}} = \Delta H_{\mathrm{f}}(\mathrm{ZnS}) = -2.0$ eV[12] to maintain the thermodynamic equilibrium between Zn, S and ZnS ($\Delta\mu_{\mathrm{Zn}} + \Delta\mu_{\mathrm{S}} = \Delta H_{\mathrm{f}}(\mathrm{ZnS})$).

Published on 03 September 2015. Downloaded by Universiteit Utrecht on 13/11/2015 09:02:06.

3. Results and discussion

3.1. Structural characterization and effects of amorphousness on the band structure

The radial distribution functions (RDF) for Zn–S, Zn–Zn and S–S pairs of the amorphous and zincblende crystals are presented in Fig. 1. In fact, CRN amorphous systems of different sizes (containing between 64 and 200 atoms) were also calculated and they have similar structural characteristics after the relaxation by DFT. The first peaks are located at the same distances in both phases, which indicates that most of the local Zn–S bonding and tetrahedral ZnS_4 configurations are preserved in the amorphous structure. The distribution of the coordination number for Zn is shown in Fig. 2, using a cut-off distance of 2.6 Å. It showed a significant amount of Zn (and S) in a-ZnS that has a "non-perfect" coordination number (3-fold instead of 4-fold coordination). This however slightly depends on the cut-off distance used for defining the bonding.

The calculations on the electronic properties of amorphous ZnS to this end will be performed on the 64-atom sample, and for comparison we used a zincblende supercell with the same number of atoms. Interestingly, the amorphous ZnS has a clean band gap (Fig. 3) despite a noticeable structural disorder and non-perfect coordination numbers. This is in contrast to many other covalent-bonded semiconductors, where non-perfect coordination often leads to mid-gap states.[47,48] In addition, Zn and S contribute to both VBM and CBM in either structure (amorphous and crystalline). In order to correct the well-known band gap underestimation by GGA, we performed additional calculations with the non-local hybrid functional (HSE06),[32] using the pre-optimized structures from the DFT+U method. The hybrid calculation yielded a band gap of 3.45 eV for zincblende ZnS, which is close to the experimental measurements (~3.5 eV).[49,50] However, a large reduction of the band gap was observed upon amorphization (2.75 eV from the HSE06 calculation). The a-ZnS density obtained by DFT+U (3.75 g cm^{-3}) is significantly lower than the corresponding zincblende ZnS value of 4.16 g cm^{-3} (the experimental value is 4.09 g cm^{-3} [51]). Despite this difference in density, the average Zn–S bond distance in the amorphous phase (d^{avg} = 2.35 Å, calculated for all 4-fold coordinated Zn) is still comparable to that in the crystal (2.32 Å). Further experimental verification is probably needed to shed light on whether the band gap reduction is caused by the "imperfectness" of the amorphous model, or is an intrinsic feature of the ZnS amorphous structure.

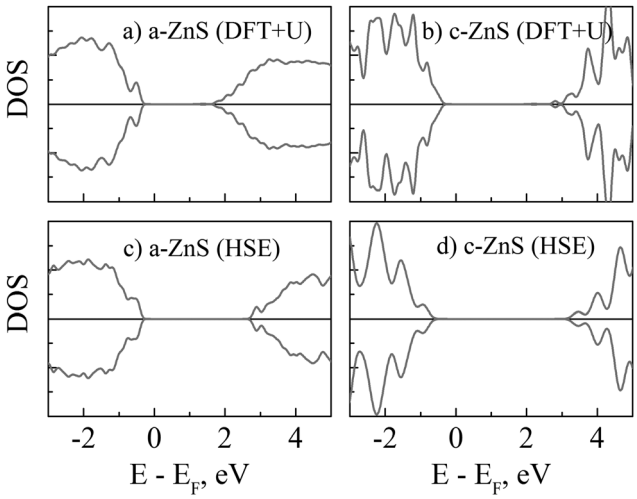

Fig. 3 Density of states of crystalline and amorphous ZnS calculated using DFT+U and HSE06. The pre-optimized structures obtained from DFT+U were used for the hybrid calculations.

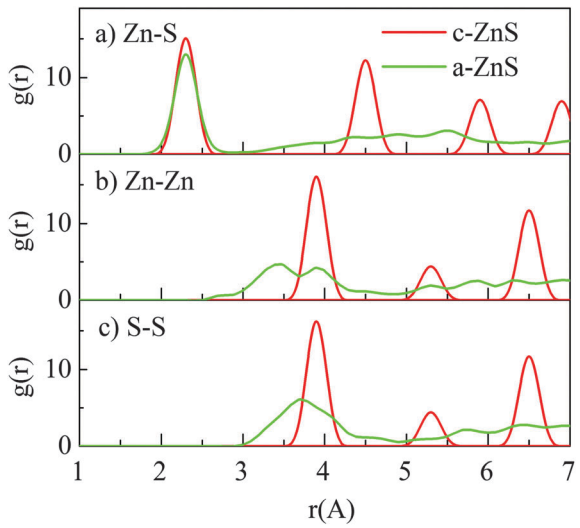

Fig. 1 Radial distribution functions $g(r)$ for (a) Zn–S, (b) Zn–Zn and (c) S–S pairs of the zincblende (c-ZnS) and amorphous (a-ZnS) zinc sulfide models.

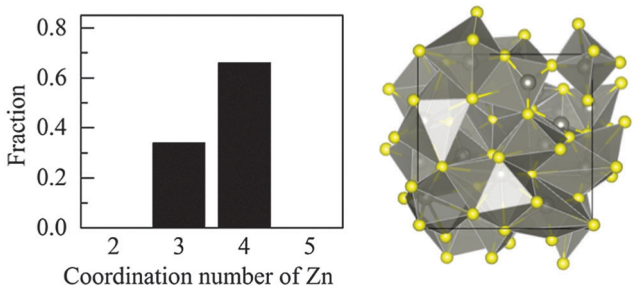

Fig. 2 Coordination number distribution of Zn (left) and the relaxed structure of the 64-atom amorphous ZnS model (right). The cutoff distance for calculating the neighbors r = 2.6 Å and DFT+U was used for the atomic relaxation after the structure was generated by the CRN method. Dark sphere – Zn and light sphere – S.

3.2. Cu doping in crystalline and amorphous ZnS

Fig. 4 displays the formation energy calculations for Cu_{Zn} (substitution of Zn by Cu) and V_S (S vacancy) defects in the amorphous and zincblende ZnS at various charge states. Note that, in the a-ZnS case there are different sites to replace Zn and/or remove S, which could yield different formation energies. The reported values in Fig. 4 are the lowest formation energy ones for the corresponding impurity species. They represent possible defect sites in an actual amorphous system. The defect sites were chosen as described in the following. It was seen that the valence

 This journal is © the Owner Societies 2015

Published on 03 September 2015. Downloaded by Universiteit Utrecht on 13/11/2015 09:02:06.

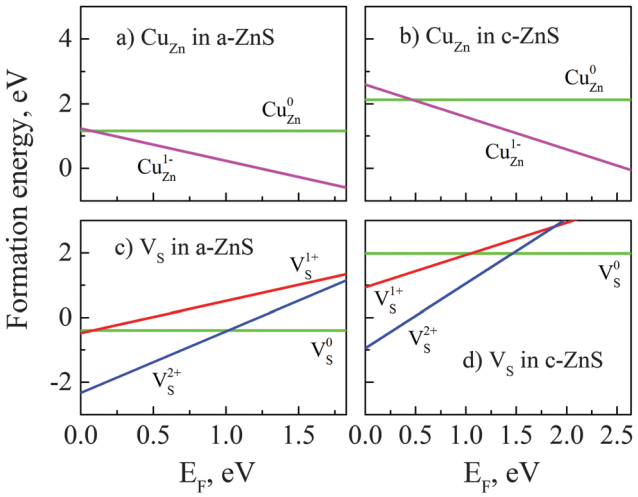

Fig. 4 Formation energy of Cu substitution (Cu_{Zn}) and the S vacancy (V_S) as a function of Fermi energy in: (a and c) amorphous ZnS and (b and d) crystalline ZnS. The crossing points show the transition energy levels between different charge states. The positive slope means the positively charged state, while the negative slope corresponds to the negatively charged state. The results (GGA+U) were calculated for Cu-rich, Zn-rich and S-poor conditions.

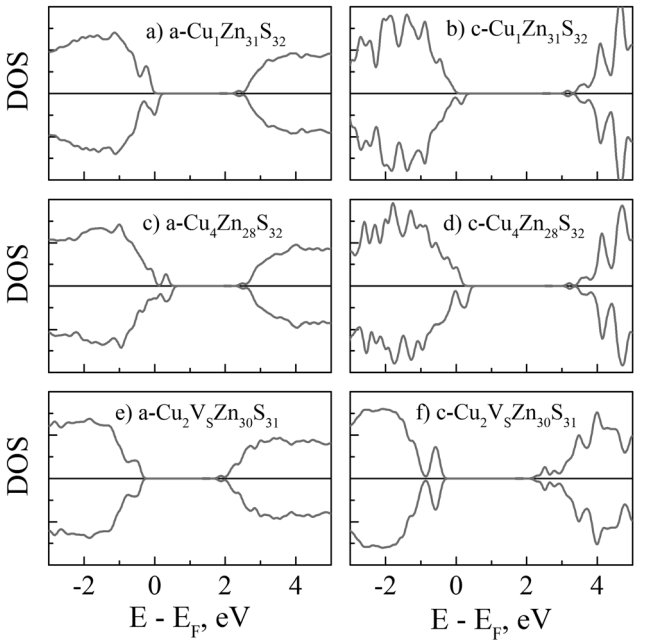

Fig. 5 Density of states of amorphous (a-ZnS) and zincblende (c-ZnS) at different Cu contents (DFT+U calculations). In figures (a and b), one Zn is replaced by Cu in the supercells. In figures (c and d), four Cu atoms substitute Zn at corners of the same Zn–S tetrahedron. In figures (e and f), the complex (of two Cu_{Zn} and the S vacancy) also belongs to the same tetrahedron configuration (as shown in Fig. 6d).

band maximum (VBM) and conduction band minimum (CBM) states of the amorphous ZnS are localized on some sulfur and zinc atoms, respectively, instead of being delocalized all over the supercell. Those Zn and S are then used as the most favorable sites for the corresponding defect formation. Our calculations indicated that they all follow the trend in which the formation of defects in a-ZnS is energetically more favorable than its crystalline counterparts. This observation is consistent with what was reported for other amorphous materials.[52] This further suggests that the Cu solubility limit could be higher in the amorphous phase. Also, the acceptor ionization level (transition energy levels from Cu_{Zn}^0 to Cu_{Zn}^{1-}, Fig. 4) is slightly shallower in a-ZnS, compared to that in c-ZnS.

Our calculations show that the substitution of Zn by Cu results in a hole in the valence band, indicating the presence of Cu^{1+} (in other notation, Cu_{Zn}^{1-}) instead of Cu^{2+}. The Fermi level is shifted into the valence band in which the shifting depth depends on the amount of Cu content (Fig. 5a–d). This electronic characterization denotes a p-type metallic conductor.[49] The density of state (DOS) calculations also showed that the incorporation of Cu only makes contributions to the valence band edge that slightly narrows the band gap (in both crystalline and amorphous systems), instead of inducing any mid-gap states.

3.3. Intrinsic charge compensation models for Cu doping: S vacancy and S–S bonding

Charge-compensated complex of an S vacancy and two substitutional Cu ($V_SCu_{Zn}Cu_{Zn}$). It is believed that the doping of Cu could be significantly enhanced if there were a mechanism to balance the charges (holes) induced by its +1 oxidation state, thus helps stabilize Cu in host lattice ZnS. Fig. 4 presents the calculations of separate V_S and Cu_{Zn}. When the Fermi energy is close to the valence band edge, the formation of V^{2+} (which can compensate the free hole carrier) in c-ZnS is not very likely (only has a rather small negative formation energy). Meanwhile, its introduction into a-ZnS is more feasible (with a large negative formation energy). Nevertheless, the possibility of defect clusters was not considered in Fig. 4. Based on experimental measurements, many such complexes have been proposed, including: two Cu_{Zn}^{1-} adjacent to a sulfur vacancy V_S^{2+}, one Cu_{Zn}^{1-} next to Cl_S^{1+} (substitution of S by Cl), and a complex of two Cu_{Zn}^{1-} and one interstitial Cu_i^{2+}.[31] Here, we will only investigate the situation of two Cu_{Zn}^{1-} adjacent to a sulfur vacancy V_S^{2+}. In Fig. 6, we present the local structural relaxation induced by the S vacancy in the zincblende system. When the sulfur atom is removed at its neutral state (V_S^0), the surrounding Zn atoms are relaxed towards the vacancy site, subsequently increasing the bond distance with

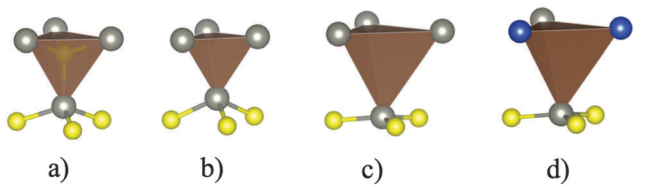

Fig. 6 Local structural relaxation induced by the S vacancy (V_S) in crystalline ZnS: (a) the perfect zinc blende structure, (b) the S vacancy at the neutral charge state V_0^S, (c) the S vacancy at its ionic state V_S^{2+}, and (d) the S vacancy in the complex with two neighboring Cu_{Zn}. In (c) and (d), both Zn and Cu are displaced away from the S vacancy and form planar configurations with three remaining S atoms. Gray sphere – Zn, blue – Cu, and yellow – S.

Published on 03 September 2015. Downloaded by Universiteit Utrecht on 13/11/2015 09:02:06.

neighboring S atoms (Fig. 6b). However, under V_S^{2+}, the neighbor Zn is instead displaced away from the vacancy and could be found near the center of the three remaining S atoms with shortened Zn–S bonds (Fig. 6c). The preference of this flat triangle arrangement over the tetrahedral symmetry is likely originated from the transition from sp^3 into the sp^2 electron configuration as two electrons are missing. The local environments are comparable between those in Fig. 6c and d, where two substitutional Cu are further introduced (which implies the Cu in the +1 charge state, or Cu_{Zn}^{1-}). The relaxation of the Zn atom to the planar configuration is not caused by the Cu substitutions *per se*, but by the loss of electrons to the two nearby Cu_{Zn} defects, thus forming an effective V_S^{2+} for the Zn-3S motif. As a result, the flat Cu-3S configurations are also formed. Our calculations showed that when this $V_SCu_{Zn}Cu_{Zn}$ complex is formed, the defect formation energy is reduced by $\Delta E_f \approx 3.8$ eV and 1.3 eV, respectively, compared to the case of separate neutral and charged Cu_{Zn} and V_S defects. This off-center displacement of Cu found by our theoretical calculations is consistent with experimental observations by Car *et al.* using the extended X-ray absorption fine structure measurements (EXAFS) of Cu doping in ZnS nanocrystals.[31] We also observed the tendency of this $V_SCu_{Zn}Cu_{Zn}$ complex formation in amorphous ZnS. However, lower ΔE_f values ($\sim$2.0 eV and 40 meV, respectively, compared to the case of separate neutral and charged defects) indicate that this mechanism of hole compensation could be less pronounced in the amorphous structure.

Covalent S–S "dumbbell" pairs. In this subsection, we will discuss another prominent mechanism for charge balance that was seen in our a-ZnS simulations. The structure optimization of the amorphous phase with high Cu doping has suggested the possibility for the presence of S–S pairs (Fig. 7c), which normally exist in crystals such as covellite CuS and pyrite-type Cu_2S.[34,35] If this S–S bond is covalent, each of these "dumbbell" units can expectedly balance the charges induced by two Cu_{Zn}^{1-} (that correspondingly produce two valence band holes). Fig. 7 displays the DOS of the amorphous supercell that contains two Cu_{Zn}, before and after the formation of a S–S bond. The S–S bond distance (Fig. 7c) was measured at approximately 2.1 Å, comparable to that in both covellite and pyrite copper sulfide.[34,35] It was shown that the original hole states disappear after the S–S bond is formed. Upon formation of a S–S dumbbell pair, two empty states start rising in the middle of the band gap and finally merge into the conduction band (Fig. 7b and c). The formation energy of this S–S bond in the amorphous structure is $E_f^{S-S} = -1.45$ eV. Due to this negative value, the formation of a $Cu_{Zn}Cu_{Zn}$(S–S) complex in a-ZnS could be automatic as its energy ($E_f^{comp} = -1.89$ eV) is smaller than that of two substitutional Cu_{Zn} without the S–S bonding pair ($E_f^{2Cu} = 2.33$ eV). These values in c-ZnS are $E_f^{S-S} = -1.20$ eV and $E_f^{comp} = -5.35$ eV, respectively. These numbers indicate that the formation of S–S dumbbell units could be more pronounced in a-ZnS and not likely in c-ZnS. Note that the introduction of S–S bonding pairs should be intrinsically easier compared to the V_S formation, since it only involves the local distortion of surrounding atoms and does not require long distance migration of S (to yield the vacancy). Our calculations using the nudged elastic band method[53] suggested that the structure relaxation (around Cu_{Zn}) to form a S–S covalent bond in a-ZnS could occur spontaneously without any energy barrier in some cases.

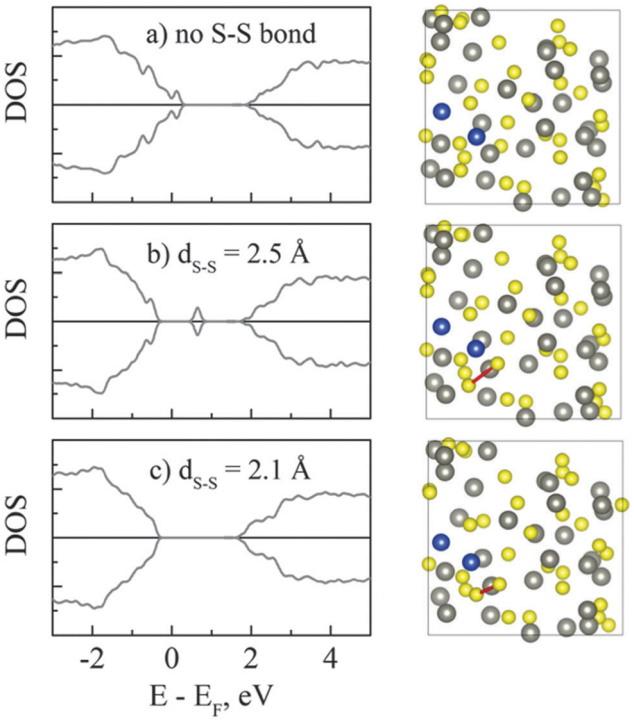

Fig. 7 The disappearance of hole states (at the VBM) by the formation of a S–S bond in the amorphous structure ($Cu_2Zn_{30}S_{32}$). Two holes exist when two substitutional Cu atoms are introduced (a), but as the S–S pair distance reduces (the red line, from (b) to (c)), those hole states rise up and disappear into the conduction band (c). Gray sphere – Zn, blue – Cu, and yellow – S.

4. Conclusions

In summary, we have investigated the Cu doping in both crystalline and amorphous zinc sulfide by the continuous random network model and density functional theory calculations. In the amorphous ZnS structure, the nearest neighbor Zn–S bonding and local tetrahedral configurations are preserved. The long-range disorder and imperfect coordination of Zn and S do not induce defect states but do reduce the band gap, and also result in the wave function localization of the band edge states. The cost of doping in a-ZnS is energetically more favorable (easier) compared to c-ZnS, probably due to the intrinsic structural disorder and bonding frustration. Each substitution of Zn by Cu introduces a valence band hole, which indicates the +1 oxidation state of Cu and expectedly makes the material a metallic conductor of p-type.

However, there are various mechanisms that could readily compensate these hole states in both crystalline and amorphous ZnS, thus reducing the likelihood of p-type doping. One is the presence of the sulfur vacancy at the 2+ charge state (V_S^{2+}) when the Fermi energy is close to the valence band edge (p-type). This is particularly true for a-ZnS. Besides, the formation of a $V_S^{2+}Cu_{Zn}^{1-}Cu_{Zn}^{1-}$ complex, which has much lower formation energy than that of separated defects, could be more prominent

 This journal is © the Owner Societies 2015

Published on 03 September 2015. Downloaded by Universiteit Utrecht on 13/11/2015 09:02:06.

in eliminating the hole carriers. In this defect complex, neighboring Cu and Zn are displaced away from the vacancy and towards the remaining S, forming a planar sp^2 configuration, which is consistent with experimental EXAFS observations.[31] In addition, another hole killing mechanism is the formation of covalent S–S bonds in a-ZnS. When the Fermi energy is near the valence band edge, we found that the formation energy of the S–S pair is negative in a-ZnS, and the spontaneous formation of this S–S dumbbell without a kinetic barrier height could be possible. While the former mechanism (V_S defect and V_S complex in c-ZnS) was already proposed by experiments,[31] the latter one (S–S pair) in a-ZnS needs further experimental investigations. All in all, we find that, while it is energetically easier to dope a-ZnS with Cu compared to c-ZnS, there are also more mechanisms to compensate the p-type hole carriers in a-ZnS.

Acknowledgements

We would like to thank Dr Shiyou Chen, Dr Jason Cooper, Dr Joel Ager, Dr Jie Ma, Dr Danylo Zherebetskyy, Rachel Woods-Robinson and Xiaojie Xu for helpful discussions. This material is based on the work performed by the Joint Center for Artificial Photosynthesis, a DOE Energy Innovation Hub, supported through the Office of Science of the U.S. Department of Energy under Award number DE-SC0004993. We use the resource of the National Energy Research Scientific Computing center (NERSC) located in Lawrence Berkeley National Laboratory.

References

1 H. Hosono, Recent progress in transparent oxide semiconductors: Materials and device application, *Thin Solid Films*, 2007, **515**(15), 6000–6014.
2 A. N. Banerjee and K. K. Chattopadhyay, Recent developments in the emerging field of crystalline p-type transparent conducting oxide thin films, *Prog. Cryst. Growth Charact. Mater.*, 2005, **50**(1–3), 52–105.
3 T. Minami, Transparent conducting oxide semiconductors for transparent electrodes, *Semicond. Sci. Technol.*, 2005, **20**(4), S35–S44.
4 D. O. Scanlon, A. Walsh and G. W. Watson, Understanding the p-type Conduction Properties of the Transparent Conducting Oxide $CuBO_2$: A Density Functional Theory Analysis, *Chem. Mater.*, 2009, **21**(19), 4568–4576.
5 T. Y. Yang, *et al.*, Preparation and application in p–n homojunction diode of p-type transparent conducting Ga-doped SnO_2 thin films, *Thin Solid Films*, 2010, **518**(19), 5542–5545.
6 A. N. Banerjee, S. W. Joo and B. K. Min, Quantum size effect in the photoluminescence properties of p-type semiconducting transparent $CuAlO_2$ nanoparticles, *J. Appl. Phys.*, 2012, **112**(11), 114329.
7 H. Kawazoe, *et al.*, p-type electrical conduction in transparent thin films of $CuAlO_2$, *Nature*, 1997, **389**(6654), 939–942.
8 A. Zunger, Practical doping principles, *Appl. Phys. Lett.*, 2003, **83**(1), 57–59.
9 S. Lany and A. Zunger, Dopability, intrinsic conductivity, and nonstoichiometry of transparent conducting oxides, *Phys. Rev. Lett.*, 2007, **98**(4), 045501.
10 S. B. Zhang, S. H. Wei and A. Zunger, Intrinsic n-type *versus* p-type doping asymmetry and the defect physics of ZnO, *Phys. Rev. B: Condens. Matter Mater. Phys.*, 2001, **63**(7), 075205.
11 H. Sato, *et al.*, Transparent Conducting P-Type Nio Thin-Films Prepared by Magnetron Sputtering, *Thin Solid Films*, 1993, **236**(1–2), 27–31.
12 A. M. Diamond, *et al.*, Copper-alloyed ZnS as a p-type transparent conducting material, *Phys. Status Solidi A*, 2012, **209**(11), 2101–2107.
13 M. S. Akhtar, *et al.*, Structural, optical, magnetic and half-metallic studies of cobalt doped ZnS thin films deposited *via* chemical bath deposition (vol. 3, p. 6755, 2015), *J. Mater. Chem. C*, 2015, **3**(27), 7228.
14 M. S. Akhtar, *et al.*, Chemical bath deposition of Fe-doped ZnS thin films: Investigations of their ferromagnetic and half-metallic properties, *Mater. Sci. Semicond. Process.*, 2015, **39**, 283–291.
15 M. S. Akhtar, *et al.*, Room temperature ferromagnetism and half metallicity in nickel doped ZnS: Experimental and DFT studies, *Mater. Chem. Phys.*, 2015, **160**, 440–446.
16 N. Revaprasadu, *et al.*, Deposition of zinc sulfide quantum dots from a single-source molecular precursor, *J. Mater. Res.*, 1999, **14**(8), 3237–3240.
17 V. Klimov, *et al.*, Linear and Nonlinear Transmission of Cuxs Quantum Dots, *Appl. Phys. Lett.*, 1995, **67**(5), 653–655.
18 R. Woods-Robinson, *et al.* Carrier scattering mechanisms in p-type transparent copper-alloyed ZnS: Crystalline *vs.* amorphous, *APS Meeting Abstracts*, 2015.
19 J. Stanley, *et al.*, Degradation and rejuvenation studies of AC electroluminescent ZnS:Cu,Cl phosphors, *J. Phys.: Condens. Matter*, 2010, **22**(5), 055301.
20 C. Corrado, *et al.*, Synthesis and Characterization of Organically Soluble Cu-Doped ZnS Nanocrystals with Br Co-activator, *J. Phys. Chem. C*, 2011, **115**(30), 14559–14570.
21 C. Corrado, *et al.*, Synthesis, Structural, and Optical Properties of Stable ZnS:Cu,Cl Nanocrystals, *J. Phys. Chem. A*, 2009, **113**(16), 3830–3839.
22 S. Gul, *et al.*, Effect of Al^{3+} Co-doping on the Dopant Local Structure, Optical Properties, and Exciton Dynamics in Cu^{+}-Doped ZnSe Nanocrystals, *ACS Nano*, 2013, **7**(10), 8680–8692.
23 H. Raebiger, S. Lany and A. Zunger, Origins of the p-type nature and cation deficiency in Cu_2O and related materials, *Phys. Rev. B: Condens. Matter Mater. Phys.*, 2007, **76**(4), 045209.
24 S. Narushima, *et al.*, A p-type amorphous oxide semiconductor and room temperature fabrication of amorphous oxide p–n heterojunction diodes, *Adv. Mater.*, 2003, **15**(17), 1409–1413.
25 H. H. Pham and L. W. Wang, Oxygen vacancy and hole conduction in amorphous TiO_2, *Phys. Chem. Chem. Phys.*, 2015, **17**(1), 541–550.
26 A. Walsh, J. L. F. Da Silva and S. H. Wei, Interplay between Order and Disorder in the High Performance of Amorphous Transparent Conducting Oxides, *Chem. Mater.*, 2009, **21**(21), 5119–5124.

Published on 03 September 2015. Downloaded by Universiteit Utrecht on 13/11/2015 09:02:06.

27 L. D. Sun and Q. Wang, PbS Quantum Dots Capped with Amorphous ZnS for Bulk Heterojunction Solar Cells: The Solvent Effect, *ACS Appl. Mater. Interfaces*, 2014, **6**(16), 14239–14246.
28 A. S. Barnard, C. A. Feigl and S. P. Russo, Morphological and phase stability of zinc blende, amorphous and mixed core–shell ZnS nanoparticles, *Nanoscale*, 2010, **2**(10), 2294–2301.
29 H. Z. Zhang, *et al.*, Water-driven structure transformation in nanoparticles at room temperature, *Nature*, 2003, **424**(6952), 1025–1029.
30 J. K. Cooper, S. Gul, S. A. Lindley, J. Yano and J. Z. Zhang, Tunable Photoluminescent Core/Shell Cu^{+}-Doped ZnSe/ZnS Quantum Dots Codoped with Al^{3+}, Ga^{3+}, or In^{3+}, *ACS Appl. Mater. Interfaces*, 2015, **7**(18), 10055–10066.
31 B. Car, *et al.*, Probing the local structure of dilute Cu dopants in fluorescent ZnS nanocrystals using EXAFS, *Nanoscale*, 2011, **3**(10), 4182–4189.
32 J. Paier, *et al.*, Screened hybrid density functionals applied to solids (vol. 124, p. 154709 2006), *J. Chem. Phys.*, 2006, **125**(24), 249901.
33 S. L. Dudarev, *et al.*, Electron-energy-loss spectra and the structural stability of nickel oxide: An LSDA+U study, *Phys. Rev. B: Condens. Matter Mater. Phys.*, 1998, **57**(3), 1505–1509.
34 H. J. Gotsis, A. C. Barnes and P. Strange, Experimental and Theoretical Investigation of the Crystal-Structure of Cus, *J. Phys.: Condens. Matter*, 1992, **4**(50), 10461–10468.
35 G. Vanderlaan, *et al.*, Oxidation-State Variations in Copper Minerals Studied with Cu 2p X-Ray Absorption-Spectroscopy, *J. Phys. Chem. Solids*, 1992, **53**(9), 1185–1190.
36 F. Wooten, K. Winer and D. Weaire, Computer-Generation of Structural Models of Amorphous Si and Ge, *Phys. Rev. Lett.*, 1985, **54**(13), 1392–1395.
37 N. Mousseau and G. T. Barkema, Fast bond-transposition algorithms for generating covalent amorphous structures, *Curr. Opin. Solid State Mater. Sci.*, 2001, **5**(6), 497–502.
38 W. Kohn and L. J. Sham, Self-Consistent Equations Including Exchange and Correlation Effects, *Phys. Rev.*, 1965, **140**(4A), 1133–1138.
39 G. Kresse and J. Furthmuller, Efficient iterative schemes for *ab initio* total-energy calculations using a plane-wave basis set, *Phys. Rev. B: Condens. Matter Mater. Phys.*, 1996, **54**(16), 11169–11186.
40 P. E. Blochl, Projector Augmented-Wave Method, *Phys. Rev. B: Condens. Matter Mater. Phys.*, 1994, **50**(24), 17953–17979.
41 J. P. Perdew, K. Burke and M. Ernzerhof, Generalized gradient approximation made simple, *Phys. Rev. Lett.*, 1996, **77**(18), 3865–3868.
42 J. P. Tang, *et al.*, First principles study on magnetic properties in ZnS doped with palladium, *Eur. Phys. J. B*, 2013, **86**(8), 362.
43 T. Miyake, *et al.*, Quasiparticle energy of semicore d electrons in ZnS: Combined LDA+U and GW approach, *Phys. Rev. B: Condens. Matter Mater. Phys.*, 2006, **74**(24), 245213.
44 L. Y. Isseroff and E. A. Carter, Importance of reference Hamiltonians containing exact exchange for accurate one-shot GW calculations of Cu_2O, *Phys. Rev. B: Condens. Matter Mater. Phys.*, 2012, **85**(23), 235142.
45 H. J. Monkhorst and J. D. Pack, Special Points for Brillouin-Zone Integrations, *Phys. Rev. B: Condens. Matter Mater. Phys.*, 1976, **13**(12), 5188–5192.
46 S. Lany and A. Zunger, Polaronic hole localization and multiple hole binding of acceptors in oxide wide-gap semiconductors, *Phys. Rev. B: Condens. Matter Mater. Phys.*, 2009, **80**(8), 085202.
47 E. B. Kandemir, *et al.*, Modeling of the atomic structure and electronic properties of amorphous GaN1-xAsx, *Comput. Mater. Sci.*, 2014, **82**, 100–106.
48 H. X. Deng, *et al.*, Electronic origin of the conductivity imbalance between covalent and ionic amorphous semiconductors, *Phys. Rev. B: Condens. Matter Mater. Phys.*, 2013, **87**(12), 125203.
49 C. I. Pearce, R. A. D. Pattrick and D. J. Vaughan, Electrical and magnetic properties of sulfides, *Sulfide Mineralolgy and Geochemistry*, 2006, **61**, 127–180.
50 J. Liu, A. X. Wei and Y. Zhao, Effect of different complexing agents on the properties of chemical-bath-deposited ZnS thin films, *J. Alloys Compd.*, 2014, **588**, 228–234.
51 B. J. Skinner, Unit-Cell Edges of Natural and Synthetic Sphalerites, *Am. Mineral.*, 1961, **46**(11–12), 1399–1411.
52 H. H. Pham and L. W. Wang, Electronic structures and current conductivities of B, C, N and F defects in amorphous titanium dioxide, *Phys. Chem. Chem. Phys.*, 2015, **17**(17), 11908–11913.
53 G. Henkelman and H. Jonsson, Improved tangent estimate in the nudged elastic band method for finding minimum energy paths and saddle points, *J. Chem. Phys.*, 2000, **113**(22), 9978–9985.

 This journal is © the Owner Societies 2015